Supporting Information

1. Synthetic details

QD550 – QD620 synthesis parameters:

The visible emitters were synthesized with a 1:4 Cu:In and 1:10 In:Zn molar ratios as described in the main text. Core QDs were grown at 230 °C for 5 min. QD550 were annealed with $ZnSt_2$ at 260 °C for 2 h. For QD570 the annealing was conducted at 230 °C and for QD620 at 210 °C.

QD650 – QD690 synthesis parameters:

The deep-red emitters were synthesized with a 1:2 Cu:In and 1:8 In:Zn molar ratios. The core QDs were grown at 210 °C for 15 min. QD650 were annealed with $ZnSt_2$ at 230 °C and QD690 at 210 °C for 2 h.

QD720 – QD750 synthesis parameters:

The NIR-emitting QDs were synthesized with a 1:1 Cu:In and 1:4 In:Zn molar ratios. Core QDs were grown at 210 °C for 45 min (QD720) or 60 min (QD750) and annealed with $ZnSt_2$ at 210 °C for 2 h.

2 mmol of $In(OAc)_3$ was used in all cases with constant amounts of all solvents as described in the main text. Longer core QD growth times typically yielded agglomerated QDs at a given Cu:In ratio and temperature. Synthetic parameters were optimized to grow as large and well-crystallized core QDs as possible and allow higher shell growth temperatures to obtain the desired emission wavelength and high quantum yields.

The final emission peak wavelength is a result of particle size-related quantum confinement effect and the substitution of core cations with Zn^{2+} producing $CuInS_2/ZnS$ solid solutions.

The hydrophilization with MPA ligands and purification procedures were identical for all QD samples and are described in the main text.

2. LED measurement setups

The SMD LEDs were measured in a diffuse setup in an integrating sphere. Color converter layers were prepared by drop-casting the polymer/QD solution directly on the LED chip and dried at 40 °C in air. The conversion efficiencies were then measured with the converter on top several minutes after turning the LED on at a forward current of 20 mA to ensure stable LED EL signal. The color converter was then removed and bare EL signal from the LED was measured to calculate the efficiency.

HP LED stability was measured directly with an optical fiber perpendicular to the LED chip surface at a distance of ca. 50 cm. Spectra were saved periodically and QD emission maximum was plotted versus time.

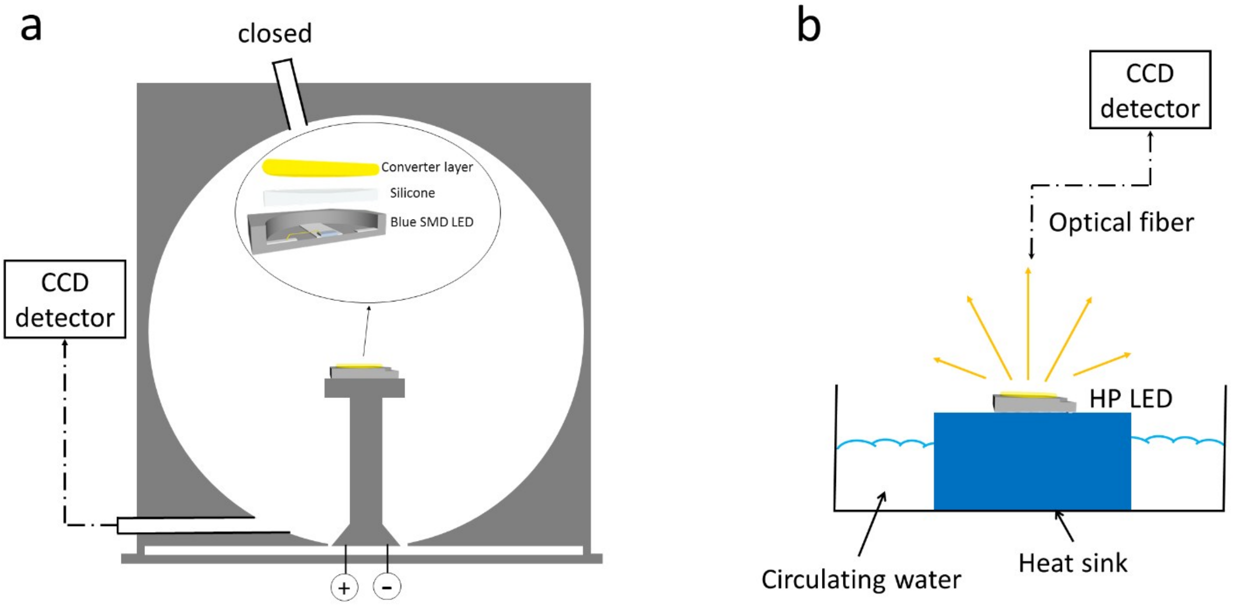

Fig. S1 Experimental setups for LED measurements: a) PTFE-lined integrating sphere and LED holder for conversion efficiencies, b) direct measurement of the EL/PL signal using fiber optics for stability tests

3. Decay times of MPA- and OA-QDs

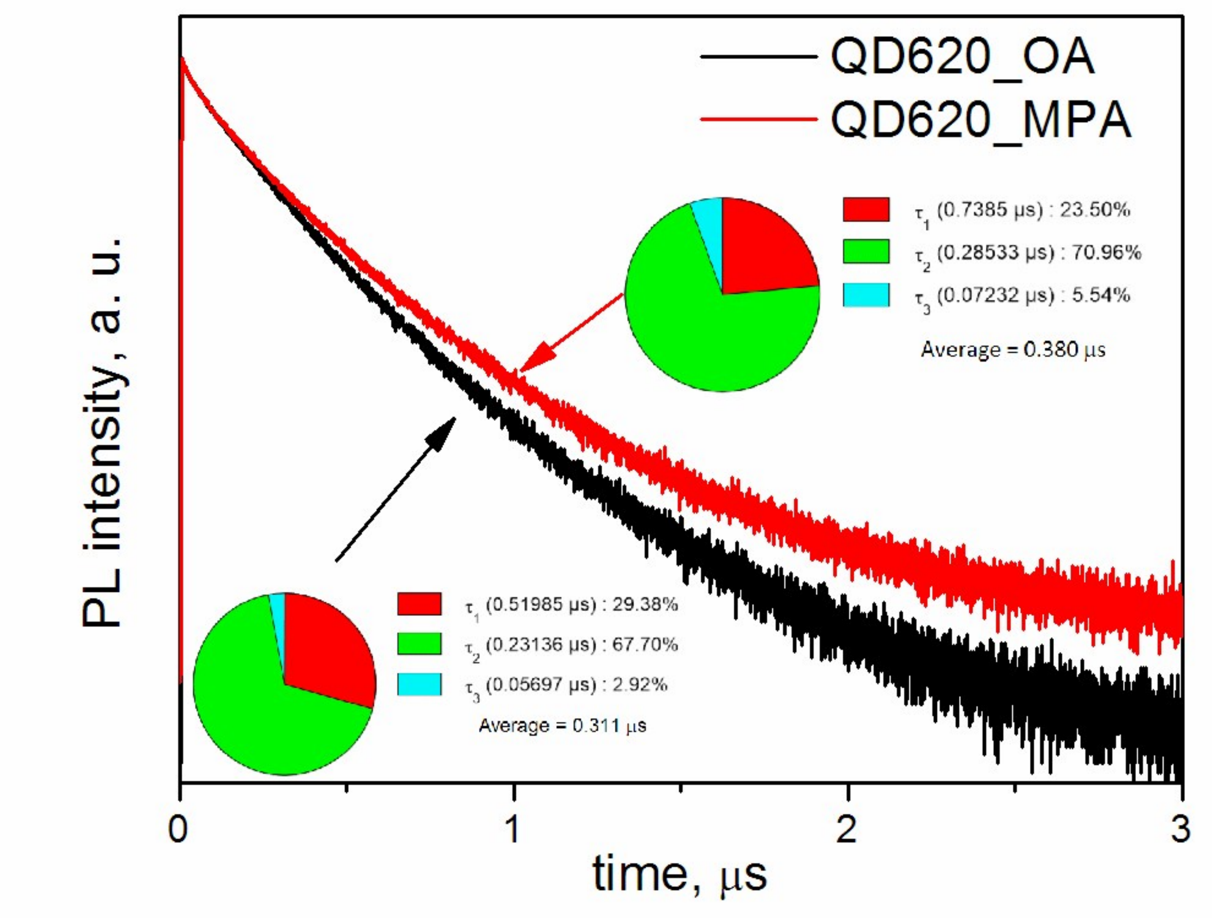

Fig. S2 Decay times of OA- and MPA-QDs. Insets represent the intensity weighted decay components.

The shortest decay component can be attributed to recombination of the surface QD states. The long decay components (300 – 500 ns) are typical for donor-acceptor pair luminescence also explaining the observed broad-band emission.

4. Infrared spectroscopy

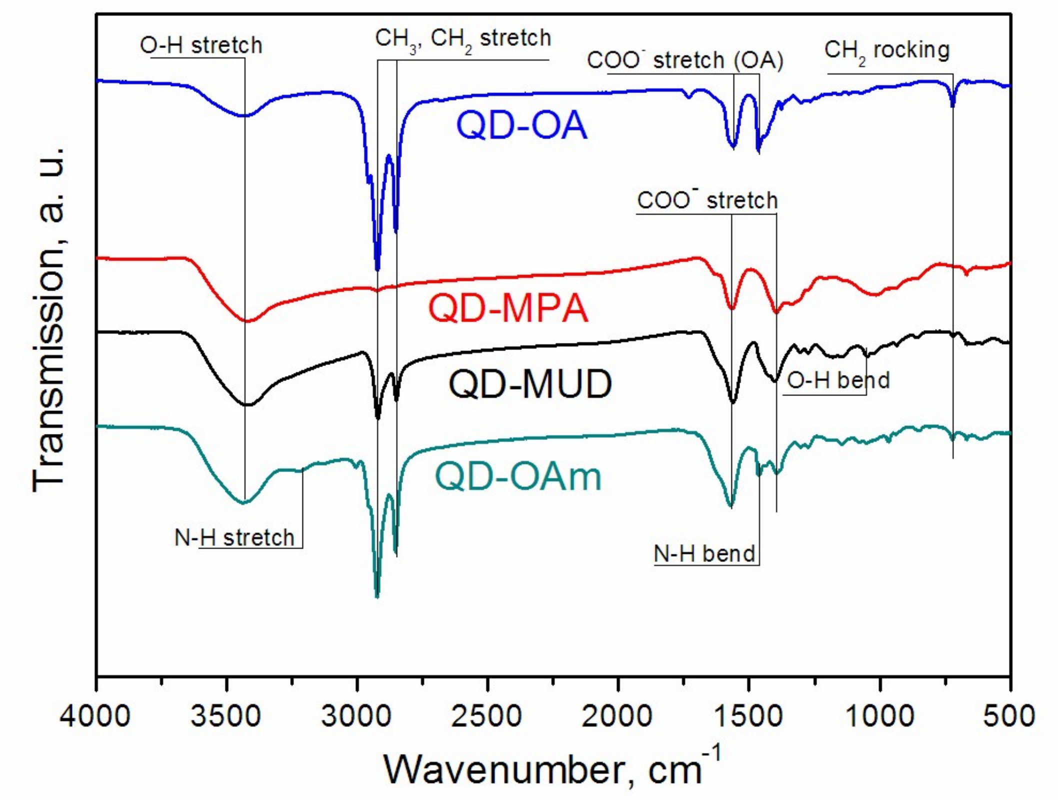

Fig. S3 FTIR spectra of QDs with various ligands.

The bands at 2923 cm^{-1} and 2852 cm^{-1} associated to long aliphatic chains and the CH_2 rocking band at 720 cm^{-1} practically vanished upon ligand exchange with MPA, while new COO^- stretching bands at 1567 cm^{-1} and 1394 cm^{-1} appeared proving complete removal of the original hydrophobic ligands. No mercaptan S-H stretch peak (~ 2550 cm^{-1}) was detected indicating complete deprotonation of the ligands. Alcohol-soluble QDs contained peaks from long aliphatic chains, OH bending (1048 cm^{-1}) as well as COO^- groups meaning that the ligand exchange was successful, but not 100 % complete. This observation explains why MUD QDs were soluble in lower alcohols only (up to ethanol). Upon MPA conjugation with OAm, N-H stretch (3150-3270 cm^{-1}) and bend (1463 cm^{-1}) bands appeared, but no band between 1250-1370 cm^{-1} attributable to covalent C-N bonding could be observed and hence the OAm-QDs were less stable than the oleic acid capped hydrophobic QDs.

5. HRTEM and XRD measurements

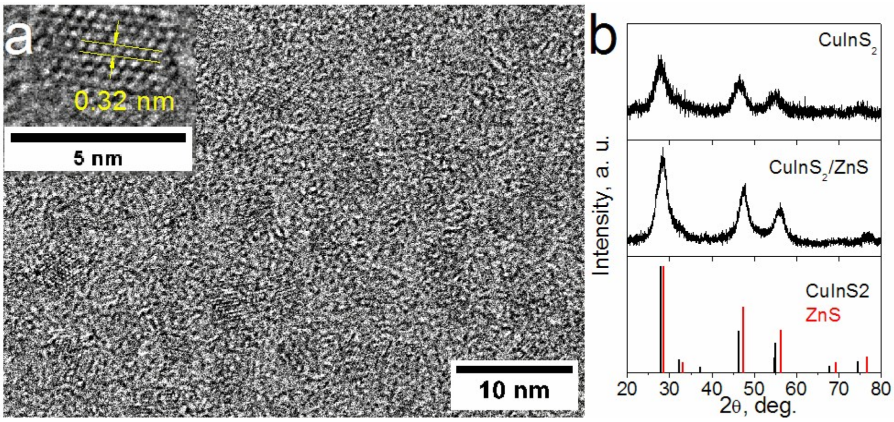

Fig. S4 a) HRTEM picture of green QDs after the ligand exchange (inset: magnified QD); b) XRD patterns of core and core/shell QDs.

HRTEM measurements revealed faceted quasi-spherical nanocrystals larger than expected from the PL peak position i.e. green luminescent particles were 4-5 nm in diameter. The increased particle size is due to heavy alloying with ZnS that makes up the bulk of the crystal. The lattice fringes were estimated to be 0.32 nm, which corresponds well with the interatomic spacing between (1 1 2) planes of the zinc blende structure.[1] XRD measurements proved that the synthesized QDs are highly crystalline with all peaks belonging to the zinc blende phase of Zn-Cu-In-S alloy. The three main reflections of chalcopyrite $CuInS_2$ attributed to (1 1 2), (2 0 4) and (3 1 2) crystal planes were shifted towards larger angles indicating small lattice strain upon annealing with $ZnSt_2$. Peak broadening due to the difference in lattice parameter of CIS and ZnS was observed but no individual peaks that could be associated with pristine ZnS were distinguishable. This observation is an evidence for the absence of individual ZnS particles but rather that the ternary and binary phases formed a solid solution. EDX results indicate that ZnS constitutes about 80-90 % of the total QD mass.

6. UV/Vis transmittance of PVP nanocomposites

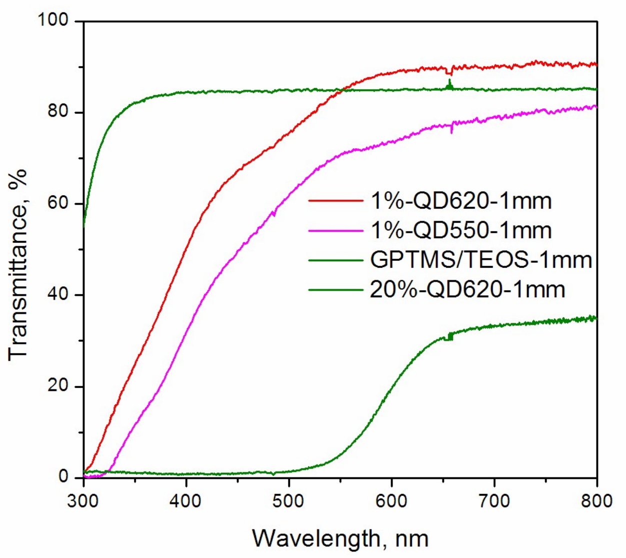

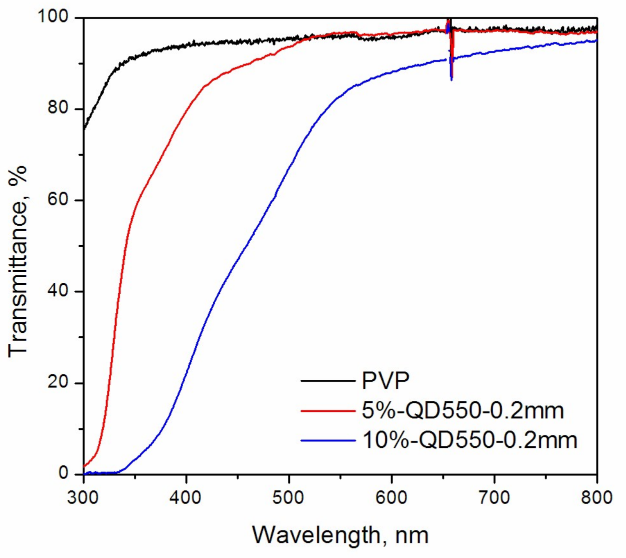

Fig. S5 Transmittance spectra of hybrid silica monoliths (top) and PVP nanocomposites (bottom) at various QD loading.

The somewhat low transmittance of the hybrids comes from light beam being defocused on the monoliths due to their uneven surface rather than from QD agglomeration within the matrix. The spectra were taken on an Ocean Optics HR4000 spectrometer equipped with an Avalight-DHS Deuterium-Halogen lamp and fiber optics.

7. SEM pictures of the sol-gel hybrids with MPA- and MUD-QDs

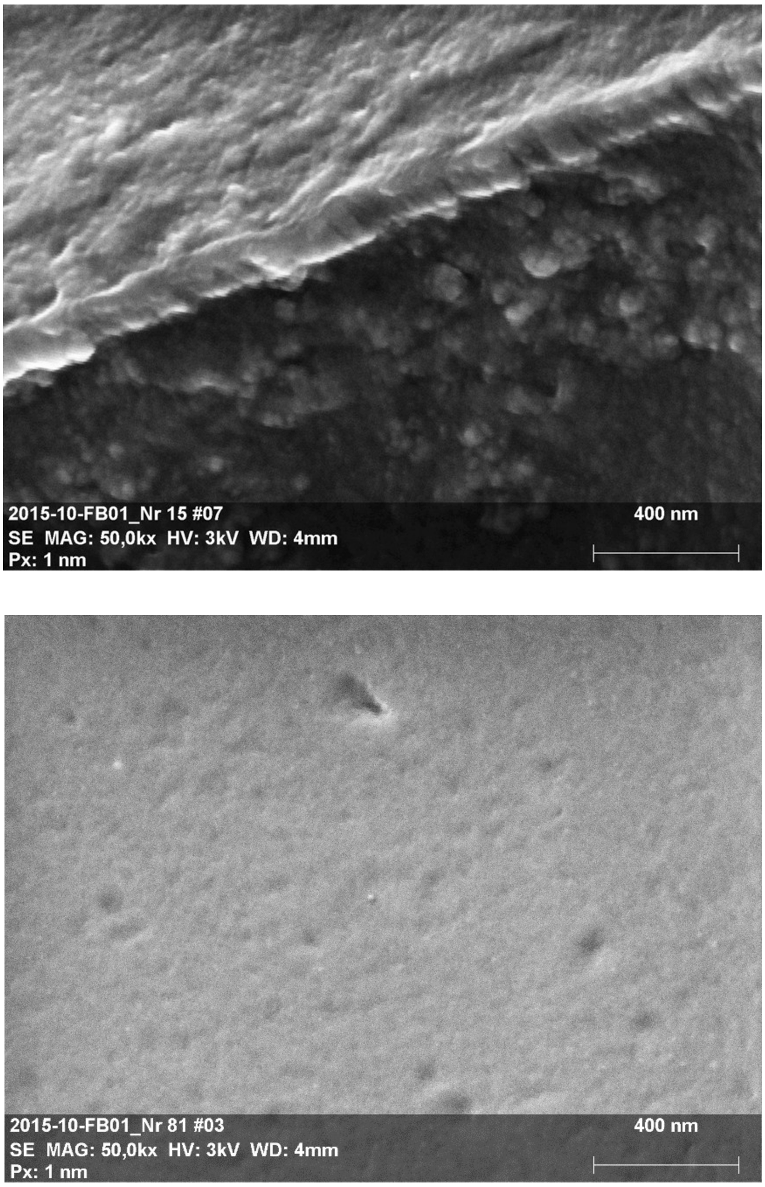

Fig. S6 SEM pictures of silica hybrids with MPA-QDs (top) and MUD-QDs (bottom). The holes are a result of focused beam damage.

8. Stability of the polymeric color converters

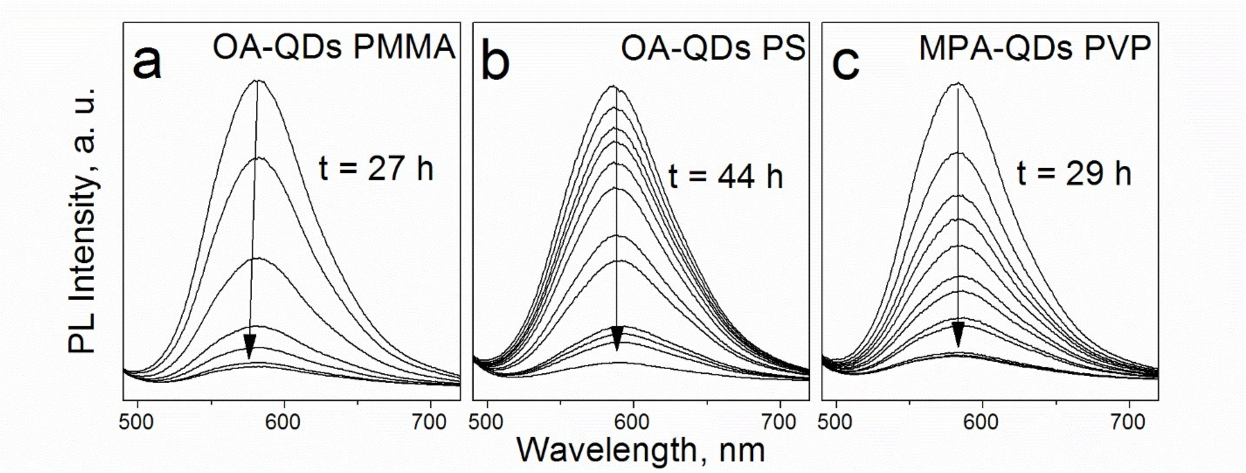

Fig. S7 Temporal evolution of down-converter emission spectra under HP LED illumination for a) PMMA, b) PS and c) PVP layers.

REFERENCES

1. F. Gong, S. Tian, B. Liu, D. Xiong and X. Zhao, *RSC Adv.*, 2014, **4**, 36875-36881.